Stress Response of Rocket Motors to Environmental Thermal Loads

Surot Thangjitham* and Robert A. Heller†
Virginia Polytechnic Institute and State University, Blacksburg, Virginia

This paper presents a general approach for the evaluation of thermal stresses and strains in solid-propellant rocket motors under outdoor storage conditions. Models for the variations of mean environmental thermal loads—ambient temperature, sky radiation, wind convection, and solar radiation—are developed by considering records of meteorological data and are used to obtain the structure's surface temperature. Numerical illustration is applied to viscoelastic stress analysis of a motor at Pheonix, Arizona.

Nomenclature

$A_k^n(B_k^n)$ = Fourier cosine (sine) coefficients for solar radiation input on the nth day; $k=1,2,...$
C_1,C_2,C_3 = constants for viscoelastic shift function
c_f = geometry constant for convection coefficient
c_1,c_2 = constants for sky temperature
D = outer diameter of the motor
D_m^a, D_k^a,$D_v^a(t)$, D_m^e, D_k^e,$D_v^e(t)$ = mean, amplitude of kth harmonic, time-varying component of air and sky temperature, respectively
$d(\theta,t)$ = solar radiation distribution function
$E_j,E(T,t),E_e,E_g$ = moduli: of the jth layer, relaxation, as $t\to\infty$, glassy
$E^*(T,\omega)$, $E'(T,\omega)$, $E''(T,\omega)$ = moduli: complex, storage, loss
$H(t),H_n(t)$, H_m^n, $H_v^n(t),H_\infty$ = solar radiation input, on the nth day, daily mean, time-varying component, yearly mean
h_n,h_m,h_y = daily peak of solar radiation input, mean, amplitude of yearly variation
j,J = layer index ($j=1,2,...,J$), number of total layers
p = shape constant for solar radiation input
Q_k, S_k = constants for A_k^n and B_k^n; $k=1,2,...$
q_k = constants, $=k\omega_d t_{2n}/\pi$; $k=1,2,...$
r,r_j = radial coordinate, outer radius of jth layer
$T^j(r,\theta,t)$, $T_s(\theta,t)$ = temperatures: of the jth layer, on the surface
$T_a(t),T_e(t),T_s(\theta,t)$ = temperatures: air, sky, surface
T_m,T_f,T_r = temperatures: motor mean, stress free, reference
t,t_p = time, period
t_{1n},t_{1m},t_{1y} = time from midnight to sunrise on the nth day, mean, amplitude of yearly variation
t_{2n},t_{2m},t_{2y} = time from sunrise to sunset on the nth day, mean, amplitude of yearly variation
$u_r^j(r,\theta,t),u_r^j(r,\theta,t)$ = displacement components of the jth layer
$V(t)$ = wind velocity
α_j = coefficient of thermal expansion of the jth layer
β_j = thermomechanical constant, $=\alpha_j E_j/2(1-\nu_j)$
$\Gamma[\cdot]$ = gamma function
γ_j = thermal diffusivity of jth layer
ϵ = thermal emissivity constant of the surface
$\epsilon(t),\epsilon_m,\epsilon_k,\epsilon_c(t)$ = strain at a point, mean, amplitude of kth harmonic, steady-state harmonic component
$e_r^j(r,\theta,t),e_\theta^j(r,\theta,t)$, $e_{r\theta}^j(r,\theta,t)$ = strain components of jth layer
$\zeta_a(t),\zeta_e(t),\zeta_h(t)$ = normalized variables for air, sky temperatures, solar radiation
η = shape parameter for relaxation modulus
θ = angular coordinate
$\vartheta,\vartheta_e,\vartheta_a,\vartheta_h$ = generalized constants: $\kappa_J/(4\epsilon\sigma T_m^3+c_f\mu_m)$, $4\epsilon\sigma\rho_e T_m^3/(4\epsilon\sigma T_m^3+c_f\mu_m)$, $\mu_m\rho_a/(4\epsilon\sigma T_m^3+c_f\mu_m)$, and $\upsilon\rho_h/2(4\epsilon\sigma T_m^3+c_f\mu_m)$, respectively
κ_j = thermal conductivity of jth layer
μ_f,μ_m = forced convection coefficient, mean of the square root of hourly wind velocity
ν_j = Poisson's ratio of jth layer
π = 3.14159...
ρ_a,ρ_e,ρ_h = normalized constants: D_m^a/T_m, $(D_m^e/T_m)^4$, and H_∞/T_m, respectively
σ = Stefan-Boltzmann constant
$\sigma(t)$ = viscoelastic stress at a point
$\sigma_r^j(r,\theta,t),\sigma_\theta^j(r,\theta,t)$, $\sigma_{r\theta}^j(r,\theta,t)$ = stress components of jth layer
τ = viscoelastic retardation time
υ = thermal absorptivity of the surface
ϕ,ϕ_k = phase angle, of kth harmonic
$\phi^j(r,\theta,t)$ = stress function of jth layer
$\chi(T)$ = viscoelastic shift function
$\psi^j(r,\theta,t),\psi_s(\theta,t)$ = normalized temperatures: of jth layer, on the surface
$\omega,\omega_d,\omega_y,\omega_k$ = circular frequency, daily, yearly, kth harmonic
∇^2 = Laplacian operator

Received March 22, 1985; revision received Sept. 30, 1985.

*Assistant Professor of Engineering Science and Mechanics.
†Professor of Engineering Science and Mechanics. Associate Fellow AIAA.

Introduction

TACTICAL solid-propellant rockets are usually stored outdoors for years without protection. Their outer surfaces are exposed to variation of various forms of environmental thermal loads—surrounding air temperature,

solar radiation, wind velocity, and sky radiation. As a result, excessive thermal stresses and strains may be induced in the motors. These in turn may produce structural damage and consequently lead to the undesirable case of structural failure.

The problem of thermal stress in solid-propellant rocket motors subjected to environmental thermal loads was first introduced by Heller et al.[1-5] and Thangjitham[6] in an effort to develop a probabilistic approach for studying their storage life. The rockets were modeled as systems of long hollow composite cylinders. Some studies[1-3] addressed these environmental thermal loads as ambient temperature applied uniformly all around the cylinder's surface, while others[4,5] considered additional asymmetric thermal loading produced by an empirical solar radiation model.

In this paper, models for the variations of mean environmental thermal loads—ambient temperature, sky radiation, wind convection, and solar radiation—are developed by considering records of meteorological data and are used to obtain the structure's surface temperature. The solid-propellant motor is modeled as a long hollow composite cylinder consisting of two stressed layers of different materials —propellant encased in a steel canister (Fig. 1). The propellant is considered to be a viscoelastic material with time- and temperature-dependent relaxation moduli. The loading conditions are considered to be uniform along the length but vary around the circumference of the motor. The effects of both thermal inertia and coupling terms will be neglected. These simplications lead to a plane strain formulation and result in two-dimensional stress analysis. Hence, solutions are applicable to the central portion of the motor away from its ends. Although the stress responses of a motor with two stressed layers are sought, the formulation herein emphasizes the general solutions for J-layered structures.

The analysis is demonstrated for Phoenix, Arizona. Hourly readings of the meteorological data are obtained from the National Oceanic and Atmospheric Administration[7] for a 25-year period (1952-1977). One standard year used in this work consists of 365 days and begins at midnight on the first day of January.

Air Temperature

It is an obvious observation that air temperature shows periodic variations. A mean air temperature variation model is assummed in the following form[4,6]:

$$T_a(t) = D_m + \sum_{k=1}^{K} D_k \cos(\omega_k t - \phi_k) \tag{1}$$

where D_m is the long-term mean air temperature, D_k and ϕ_k the amplitude and phase angle, respectively, corresponding to the circular frequency ω_k, and K the number of the dominant harmonics.

Table 1 tabulates the values for D_m, D_k, and ϕ_k of the first four most dominant frequencies for the air temperature process at Phoenix obtained by the method of least-squares regression. The maximum temperature variation is found to follow an annual cycle; the warmest day is on the 202nd day of the year. The maximum daily temperature occurs at approximately 4 p.m.

Solar Radiation

The Earth's daily rotation about its tilted axis and the annual revolution around the sun account for the distribution of solar radiation over the Earth's surface and the changing length of daylight hours. The diurnal variation of solar radiation is obvious. At night, the structure is on the shadow side of the Earth, therefore, no direct solar radiant energy is received. During the day, however, solar radiation intensity gradually increases with time before attaining its daily peak in the midafternoon and decreases with time, approaching zero, in the evening. To describe this actual change, the following model is proposed for the daily variation of solar radiation input, $H_n(t)$, on the nth day.[6]

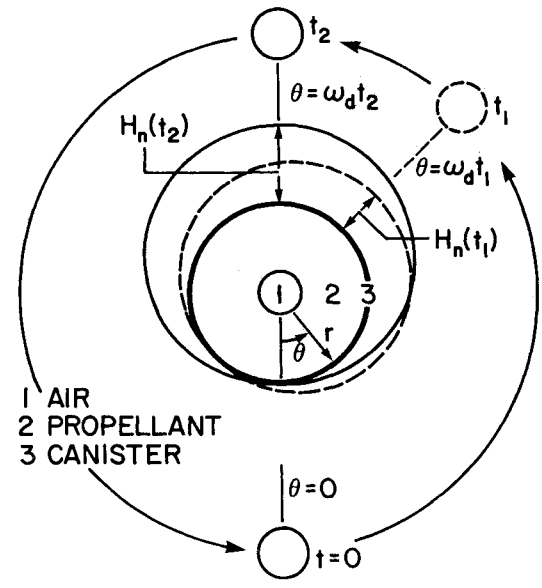

Fig. 1 Configuration of the solid-propellant motor and surface distributions of solar radiation input at various hours of a day.

$$H_n(t) = \begin{cases} 0, & 0 \le t \le t_{1n} \\ h_n \sin^p\left[\pi\left(\dfrac{t-t_{1n}}{t_{2n}}\right)\right], & t_{1n} \le t \le t_{1n}+t_{2n} \\ 0, & t_{1n}+t_{2n} \le t \le 24 \end{cases} \tag{2}$$

where h_n is the daily peak of solar radiation input, t_{1n} the time from midnight to sunrise, t_{2n} the hours from sunrise to sunset (daylight), and p a shape constant.

In order to obtain the daily values for h_n, t_{1n}, and t_{2n}, the following expressions are assumed:[6]

$$h_n = h_m + h_y \cos(24n\omega_y - \phi_h) \tag{3}$$

$$t_{1n} = t_{1m} + t_{1y} \cos(24n\omega_y - \phi_1) \tag{4}$$

$$t_{2n} = t_{2m} + t_{2y} \cos(24n\omega_y - \phi_2) \tag{5}$$

where h_m, t_{1m}, and t_{2m} are the long-term mean values for the daily peak, hours from midnight to sunrise, and hours of daylight, respectively. h_y and ϕ_h, t_{1y} and ϕ_1, and t_{2y} and ϕ_2 are the amplitudes and phases of the respective variables, and $\omega_y = 2\pi/8760$ rad/h.

Table 1 tabulates the means, amplitudes, and phase angles for h_n, t_{1n}, and t_{2n}, and the shape constant at the Phoenix site obtained by the method of least-squares regression. The resulting model is plotted for comparison with measured data in Fig. 2.

Sky Radiation

In addition to global solar radiation, the structure's surface also receives radiant energy from the sky. In the calculation of radiant energy emitted by the sky, the sky is considered to be a blackbody at some equivalent sky temperature, $T_e(t)$, so that the long-wave radiation received by the structure's surface facing the sky is given by the Stefan-Boltzmann law. This equivalent blackbody sky temperature accounts for the fact that the atmosphere is not at a uniform temperature. Long-wave radiation exchange between the structure's surface and the sky occurs.

Idso and Jackson[8] introduced the relation between the equivalent sky temperature, T_e, and air temperature, T_a, in the following form:

$$T_e = \{1 - c_1 \exp[-c_2(273.15 - T_a)^2]\}^{0.25} T_a \tag{6}$$

where T_a and T_e are both in degrees Kelvin, and c_1 and c_2 are given as 0.261 and 0.777×10^{-3}, respectively.

Table 1 Characteristics of environmental thermal loads at Phoenix, AZ

Period, h	Amplitude, °C/°F	Phase angle, h
Air temperature, mean (°C/°F) = 21.40/70.51		
8760.0	11.37/20.46	4840.24
24.0	6.58/11.84	15.96
4380.0	1.03/ 1.85	1443.87
12.0	1.02/ 1.84	1.71
Equivalent sky temperature, mean (°C/°F) = 7.63/45.74		
8760.0	16.12/29.02	4844.93
24.0	9.25/16.64	15.94
4380.0	1.51/2.72	1331.39
12.0	1.42/2.57	1.78

	Mean	Amplitude	Phase angle, day
Solar radiation			
Midnight-sunrise, t_1, h	6.10	1.02	358
Daylight, t_2, h	12.81	2.11	176
Daily peak, kJ/m^2-h	2855.28	919.83	176
Btu/ft^2-h	251.59	81.05	
Shape constant, p	1.626		

The derived time series for the equivalent sky temperature is obtained by simply substituting the hourly air temperature readings into Eq. (6). Using a model similar to that used for air temperature, Table 1 gives values for the mean, amplitudes, and phases for the first four dominant frequencies. It appears that there is approximately 24°F difference between the mean air and sky temperatures.

Wind Velocity

Wind velocity affects the energy balance of the structure's surface by inducing forced convection. In general practice, wind velocity enters the energy balance equation in terms of the forced convection coefficient, $\mu_f(t)$. Together with the difference between air and surface temperatures, the amount of heat energy transferred can be obtained.

Most recently, Ulrich[9] proposed an empirical expression for μ_f applied to cylindrical bodies as

$$\mu_f = 0.6[V/D]^{0.5} \quad \text{for} \quad VD < 6$$
$$= 1.0[V/D]^{0.5} \quad \text{for} \quad VD \geq 6 \tag{7}$$

where $V(t)$ is wind speed in feet per second, D is the outer diameter of the cylinder in feet, and μ_f is in Btu/ft^2-h-°F.

It is an obvious observation that wind velocity is random in nature. As a result, the induced convection coefficient is a random process. In this paper, however, the convection coefficient is assumed to be constant and to be equal to the average value obtained via a single formulation represented by the second expression of Eq. (7). Therefore,

$$\mu_f = c_f \mu_m \tag{8}$$

where μ_m is the average of the square root of the hourly wind velocity readings and is found to be 2.597 Btu/ft^2-h-°F for Phoenix, and $c_f = 1/\sqrt{D}$ is a dimensionless geometry-dependent constant ($\mu_m = 8.141$ W/m^2-K and $c_f = 1/\sqrt{D}$, where D is in meters).

Surface Temperature

For a structure with its surface exposed to an outdoor environment, the boundary condition describing surface temperature is quite complicated and is, in fact, highly nonlinear. At night, the surface temperature is influenced by three major forms of heat transfer: convection of heat due to movement of the surrounding air, conduction of heat from the surface into the interior parts of the structure, and long-wave radiation heat exchange between the surface and the sky. In the daytime, additional solar radiant energy is applied to the surface. The heat exchange relation between the structure's surface and the surrounding environment is given as[6]

$$\kappa_J \frac{\partial T_s}{\partial r} + \epsilon\sigma(T_s^4 - T_e^4) + c_f\mu_m(T_s - T_a) = \upsilon H(t)\mathrm{d}(\theta, t) \tag{9}$$

where T_s, T_a, and T_e are the absolute surface, air, and sky temperatures, respectively, κ_J, ϵ, and υ are the thermal conductivity, emissivity, and absorptivity of the cylinder's surface, and $\sigma = 0.1714 \times 10^{-8}$ Btu/ft^2-h-°R (5.6697×10^{-8} W/m^2-°K) is the Stefan-Boltzmann constant.

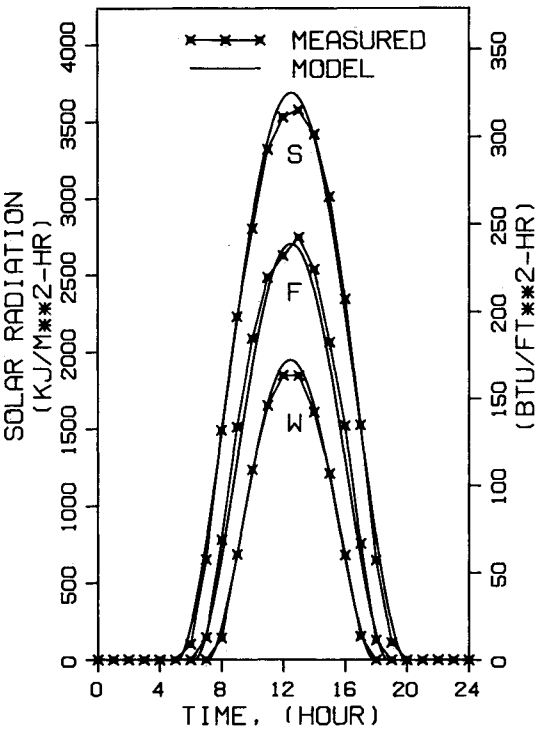

Fig. 2 Average hourly readings of global radiation on various days of the year at Phoenix, AZ (S, summer; F, fall; W, winter).

Fourier Series for Daily Solar Radiation Input

Solar radiation introduces loading complexities into the surface boundary condition, Eq. (9). Within a given day, the amount of solar radiant energy received by the cylinder's surface varies significantly. It attains its daily peak in midafternoon and vanishes at night.

For analytical ease, it is expedient to rewrite the daily variation of solar radiation input, Eq. (2), into a Fourier series representation in terms the diurnal frequency, $\omega_d = 2\pi/24$ rad/h, as

$$H_n(t) = H_m^n + H_v^n(t) = H_m^n + \sum_{k=1}^{\infty} [A_k^n \cos(k\omega_d t) + B_k^n \sin(k\omega_d t)] \tag{10}$$

where H_m^n is the mean value, A_k^n and B_k^n ($k = 1,2,\ldots$) are the Fourier coefficients, and are defined as[6]

$$H_m^n = t_{2n} h_n 2^p \Gamma^2 \left[\frac{p+1}{2}\right] \Big/ 24\pi p \Gamma[p] \tag{11}$$

$$A_k^n = \frac{t_{2n}}{12\pi} h_n [Q_k \cos(k\omega_d t_{1n}) - S_k \sin(k\omega_d t_{1n})] \tag{12}$$

$$B_k^n = \frac{t_{2n}}{12\pi} h_n [Q_k \sin(k\omega_d t_{1n}) + S_k \cos(k\omega_d t_{1n})] \tag{13}$$

where $\Gamma[\cdot]$ is the gamma function and S_k and Q_k are given as

$$S_k = \frac{2^{(2-p)}\pi p\Gamma[p]\sin[(\pi/2)q_k]}{(p^2-q_k^2)\Gamma[(p+q_k)/2]\Gamma[(p-q_k)/2]},\quad p>q_k$$

$$= \frac{-2^{(1-p)}p(q_k-p)\Gamma[p]\Gamma[(q_k-p)/2]\sin[(\pi/2)q_k]\sin[(\pi/2)(q_k-p)]}{(p^2-q_k^2)\Gamma[(p+q_k)/2]};\quad p<q_k \tag{14}$$

$$Q_k = \frac{2^{(2-p)}\pi p\Gamma[p]\cos[(\pi/2)q_k]}{(p^2-q_k^2)\Gamma[(p+q_k)/2]\Gamma[(p-q_k)/2]},\quad p>q_k$$

$$= \frac{-2^{(1-p)}p(q_k-p)\Gamma[p]\Gamma[(q_k-p)/2]\cos[(\pi/2)q_k]\sin[(\pi/2)(q_k-p)]}{(p^2-q_k^2)\Gamma[(p+q_k)/2]};\quad p<q_k \tag{15}$$

and $q_k = k\omega_d t_{2n}/\pi$.

It was shown earlier that the constants h_n, t_{1n}, and t_{2n} vary slowly from day to day and follow an annual cycle. Consequently, the daily Fourier coefficients given by Eqs. (11-13) will also have a similar trend of variation.

Solar Radiation Intensity Distribution Function

In addition to the annual variation of the daily peak value, the intensity of solar radiation input varies depending upon the position of the sun with respect to the cylinder's surface. In this study, the motor is assumed to be lying on the ground with the sun rotating in a plane perpendicular to the longitudinal axis of the cylinder. At midnight, the center of the sun coincides with the line $\theta = 0$ (point of contact with the ground). The sun completes its revolution in the counterclockwise direction within a 24-h period (Fig. 1).

Under these circumstances, the top ($\theta = 180$ deg) of the cylinder faces the sun at noon, while the regions where θ are in the neighborhood of 90 and 270 deg face the sun in the morning and evening, respectively. Therefore, within a day, the distribution of solar radiation intensity on the cylinder's surface for given time t and angle θ is assumed to be of the following form:

$$\mathrm{d}(\theta,t) = \tfrac{1}{2}[1+\cos(\theta-\omega_d t)] \tag{16}$$

According to Eq. (16), at time t, points on the cylinder's surface with $\theta = \omega_d t$ and $\omega_d t + \pi$ receive the maximum ($H_n(t)$) and minimum (zero) solar radiation input, respectively, while points with $\theta = \omega_d t + \pi/2$ and $\omega_d t - \pi/2$ receive the average value.

Linearized Surface Boundary Condition

In addition to being highly nonlinear, the surface boundary condition is subject to loading complexities. Air and equivalent sky temperatures contain both high- (diurnal) and low- (annual) frequency variations, while solar radiation gives only high-frequency effects. Furthermore, due to the continuous change in the angular position of the sun, the solar radiant energy is asymmetrically applied to the cylinder's surface.

In order to obtain an approximate relation between the energy on the cylinder's surface and that of the surrounding environment, the following normalized variables are introduced:

$$T(r,\theta,t) = T_m[1+\psi(r,\theta,t)] \tag{17}$$

$$T_a(t) = D_m^a[1+\zeta_a(t)] \tag{18}$$

$$T_e(t) = D_m^e[1+\zeta_e(t)] \tag{19}$$

$$H(t) = H_\infty[1+\zeta_h(t)] \tag{20}$$

where T_m is the long-term mean absolute temperature of the structure, and D_m^a and D_m^e the mean absolute air and sky temperatures, respectively. H_∞ is the long-term mean solar radiation intensity defined as

$$H_\infty = h_m t_{2m} 2^p \Gamma^2\left[\frac{p+1}{2}\right]\Big/ 24\pi p\Gamma[p] \tag{21}$$

and $\zeta_a(t)$, $\zeta_e(t)$, and $\zeta_h(t)$ are defined as

$$\zeta_a(t) = D_v^a(t)/D_m^a \tag{22}$$

$$\zeta_e(t) = D_v^e(t)/D_m^e \tag{23}$$

$$\zeta_h(t) = [H(t)-H_\infty]/H_\infty \tag{24}$$

$D_v^a(t)$ and $D_v^e(t)$ are the cyclic components of the air and sky temperatures, respectively.

Substituting Eqs. (17-20) into Eq. (9), there results a surface boundary condition in terms of the normalized variables as

$$\kappa_f\frac{\partial\psi_s}{\partial r} + \epsilon\sigma T_m^3[(1+\psi_s)^4 - \rho_e(1+\zeta_e)^4] + c_f\mu_m[(1+\psi_s) - \rho_a(1+\zeta_a)] = \tfrac{1}{2}v\rho_h(1+\zeta_h)[1+\cos(\theta-\omega_d t)] \tag{25}$$

where $\rho_e = (D_m^e/T_m)^4$, $\rho_a = D_m^a/T_m$, and $\rho_h = H_\infty/T_m$, and the subscript s indicates the value of the function on the cylinder's surface.

Constant Mean Temperature

The long-term mean response temperature of the structure is obtained by grouping the nonvarying terms in Eq. (25). As a result, writing in terms of the original variables, the mean response temperature is expressed as

$$\epsilon\sigma T_m^4 + c_f\mu_m T_m = \tfrac{1}{2}vH_\infty + \epsilon\sigma(D_m^e)^4 + c_f\mu_m D_m^a \tag{26}$$

Due to the additional solar radiant energy, the mean response temperature is usually higher than the mean air temperature. However, in the case when solar radiation is absent the mean response temperature is slightly lower than the mean air temperature. This results because the mean sky temperature is normally lower than the mean air temperature. Therefore, through its surface the cylinder emits radiation into the sky at night.

Solutions for Cyclicly Varying Components

Upon obtaining the mean response temperature, the boundary condition, Eq. (25), is reduced to a form containing only terms involving cycling variations and is written as

$$\kappa_f\frac{\partial\psi_s}{\partial r} + \epsilon\sigma T_m^3[4\psi_s + 6\psi_s^2 + 4\psi_s^4 + \psi_s^4] - \epsilon\sigma\rho_e T_m^3[4\zeta_e + 6\zeta_e^2 + 4\zeta_e^3 + \zeta_e^4] + c_f\mu_m[\psi_s - \rho_a\zeta_a] = \tfrac{1}{2}v\rho_h[\zeta_h + (1+\zeta_h)\cos(\theta-\omega_d t)] \tag{27}$$

For a structure with its surface exposed to outdoor environmental thermal loads, its temperature is most affected by the variation of the surrounding air temperature. Especially at night and in the early morning, the surface and air temperatures are almost identical. In midafternoon, due to the daily peak of the solar radiation, both temperatures may experience significant differences. This condition is, however, sustained only for a short period of time and is contained within a small region around the top ($\theta = 180$ deg) of the cylinder.

Therefore, in order to obtain a simple linear relation between the surface temperature and the environmental thermal loads, the variation of the surface temperature is assumed to be of the same order as that of the air temperature. Since ψ_s and ζ_e are small, a first-order approximation can be obtained by neglecting higher order terms involving ψ_s and ζ_e. Consequently, there results a set of linearized boundary conditions as

$$\vartheta \frac{\partial \psi_s}{\partial r} + \psi_s = \vartheta_e \zeta_e + \vartheta_a \zeta_a + \vartheta_h [\zeta_h + (1+\zeta_h)\cos(\theta - \omega_d t)] \quad (28)$$

where ϑ, ϑ_e, ϑ_a, and ϑ_h are defined as

$$\vartheta = \kappa_J / (4\epsilon\sigma T_m^3 + c_f \mu_m) \quad (29)$$

$$\vartheta_e = 4\epsilon\sigma\rho_e T_m^3 / (4\epsilon\sigma T_m^3 + c_f \mu_m) \quad (30)$$

$$\vartheta_a = \mu_m \rho_a / (4\epsilon\sigma T_m^3 + c_f \mu_m) \quad (31)$$

$$\vartheta_h = \upsilon\rho_h / 2(4\epsilon\sigma T_m^3 + c_f \mu_m) \quad (32)$$

Although the boundary condition, Eq. (28), is linear, the complexity of the solar radiation term gives rise to analytical difficulties. The solar radiation loading function, $H(t)$, is defined explicitly in terms of daily variation, Eq. (2). Its characteristics, such as the daily peak and loading duration, vary depending upon a given day of the year. In terms of the Fourier series representation, Eq. (10), these changes are included in the daily coefficients—Eqs. (11-13). Therefore, the daily coefficients can be considered as slow time-varying functions following an annual cycle. Because the annual frequency of variation is negligible when compared to the diurnal frequency—principal frequency of the Fourier representation—the surface temperature variation induced by solar radiation on a given day can be obtained directly using the corresponding daily Fourier series.

In order to obtain the complete solution for the boundary-value problem, it is further necessary to expand the solar radiation loading term into the sum of various independent harmonics so that the method of complex frequency-response functions can be utilized.[6] To accomplish this, the trigonometric identities converting products into sums are employed.

Interior Temperature Distribution

In addition to the surface boundary condition provided by Eq. (28), the interior normalized temperature distribution function, $\psi^j(r,\theta,t) = [T^j(r,\theta,t) - T_m]/T_m$, of a given jth layer must also satisfy the linear Fourier heat conduction equation (with uniform temperature along the length of the cylinder and without the presence of a heat source)

$$\nabla^2 \psi^j(r,\theta,t) = \frac{1}{\gamma_j} \frac{\partial \psi^j}{\partial t}(r,\theta,t) \quad (33)$$

and the continuity conditions on temperature and heat flux at the interface of two adjacent layers

at $r = 0$:

$$\psi^1(r,\theta,t) \text{ is finite} \quad (34)$$

at $r = r_j$ $(j = 1,2,3,\ldots,J\text{-}1)$:

$$\psi^j(r,\theta,t) = \psi^{j+1}(r,\theta,t) \quad (35)$$

$$\kappa_j \frac{\partial \psi^j}{\partial r}(r,\theta,t) = \kappa_{j+1} \frac{\partial \psi^{j+1}}{\partial r}(r,\theta,t) \quad (36)$$

at $r = r_J$:

$$\psi^J(r,\theta,t) = \psi_s(\theta,t) \quad (37)$$

where ∇^2 indicates the Laplacian operator, γ_j and κ_j are the thermal diffusivity and conductivity of the jth layer $(j = 1,2,\ldots J)$, respectively, and J is the total number of layers.

Because the variations of environmental thermal loads are cyclic in nature, the method of complex frequency-response functions may be used in obtaining the analytical solutions for temperature distributions in the structure. The complete solutions for the above boundary-value problems can be found in Ref. 6, therefore the analysis will not be repeated here.

Using the geometric parameters and thermal properties shown in Table 2, Fig. 3 compares the surface heat energy [terms involving T_s in Eq. (9)] as a result of using the approximated surface temperature to the actual energy provided by the environmental loads at Phoenix. It appears that they agree quite well—especially during the night hours in the summer and the entire day in the winter. In the midafternoon of a summer day, however, the surface energy at the top of the cylinder ($\theta = 180$ deg) is slightly overestimated. This error can be reduced by increasing the order of approximation. It can be shown that, in the case where the solar radiation loading is uniformly applied to the cylinder's surface $[d(\theta,t) = 1]$, the difference between linear and second-order approximations of the surface temperature is of the order of 3-5°F, depending on the day of the year.[6] This difference is expected to be smaller for the loading conditions at hand. However, for practical purposes, such a deviation may be considered insignificant. Therefore, the linearized boundary condition relating the cylinder's surface temperature to the environmental thermal loads is used.

Figure 4 compares the daily variations of surface, air, and bore temperatures at various angular positions for a typical winter day in Phoenix.

Table 2 Geometric and thermomechanical parameters

Layer No., j Material	1 Air	2 Propellant	3 Canister
Outer radius, r_j			
in.	6.000	18.000	18.125
cm	15.240	45.720	46.038
Conductivity, κ_j			
Btu/ft-°F-h	0.0142	0.2800	14.60
W/m-K	0.0246	0.4843	25.25
Diffusivity, γ_j			
$in.^2/h$	106.28	1.5000	49.04
cm^2/h	658.68	9.6774	319.40
Emissivity, ϵ	—	—	0.5
Absorptivity, υ	—	—	0.5
Stress-free temperature, T_f			
°F	—	185	185
°C	—	85	85
Glassy modulus, E_g			
psi	—	150,000	30.0×10^6
kN/m^2	—	1,034,200	20.7×10^{10}
Relaxed modulus, E_e			
psi	—	450	30.0×10^6
kN/m^2	—	3100	20.7×10^{10}
Retardation time, τ, min	—	1.0×10^{-10}	—
Shape parameter, η	—	0.25	—
Poisson's ratio, ν_j	—	0.49	0.25
Coefficient of thermal expansion, α_j			
in./in./°F	—	6.00×10^{-5}	6.50×10^{-6}
cm/cm/°C	—	1.08×10^{-4}	1.17×10^{-5}

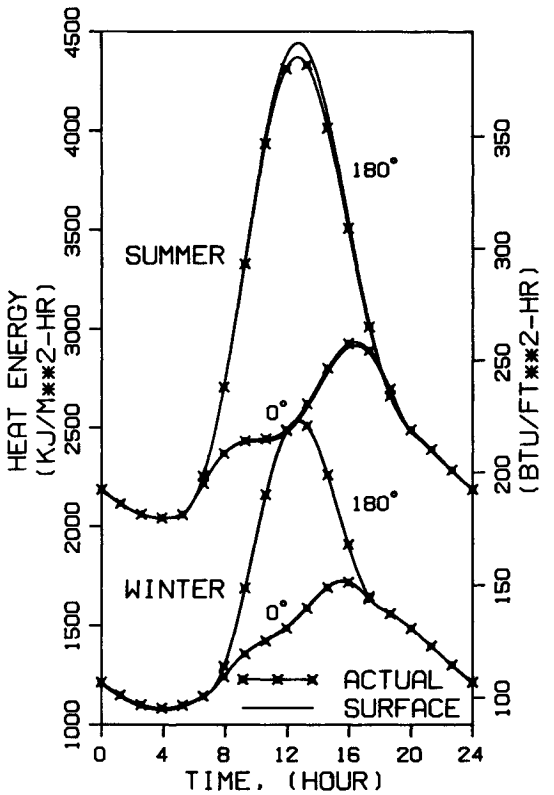

Fig. 3 Comparisons of the actual environmental and approximated heat energy on the cylinder surface at Phoenix, AZ.

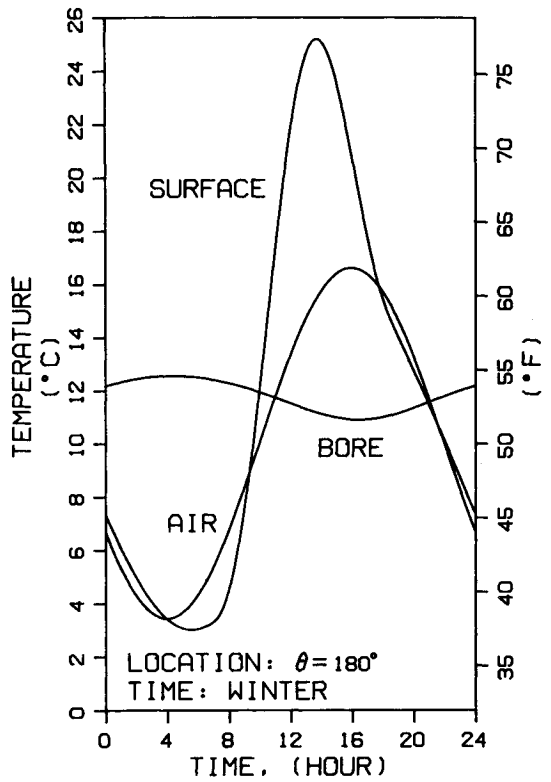

Fig. 4 Daily variation of surface, air, and bore temperatures at $\theta = 180°$ for a typical winter day at Phoenix, AZ.

Thermal Stress Analysis

For plane strain conditions, the compatibility equation for a linear thermoelasticity problem within the jth layer, expressed in terms of a stress function, $\phi^j(r,\theta,t)$, is written as[10,11]

$$\nabla^2[\nabla^2\phi^j(r,\theta,t) + 2\beta_j T^j(r,\phi,t)] = 0 \tag{38}$$

where $\beta_j = \alpha_j E_j/2(1-\nu_j)$ and α_j, ν_j, and E_j are the linear coefficient of thermal expansion, Poisson's ratio, and the modulus of elasticity, respectively.

In terms of a stress function, the stresses within each layer are calculated by the following relationships[10,11]:

$$\sigma_r^j = \frac{1}{r}\left[\frac{\partial\phi^j}{\partial r} + \frac{1}{r}\frac{\partial^2\phi^j}{\partial\theta^2}\right] \tag{39}$$

$$\sigma_\theta^j = \frac{\partial^2\phi^j}{\partial r^2} \tag{40}$$

$$\sigma_{r\theta}^j = -\frac{\partial}{\partial r}\left[\frac{1}{r}\frac{\partial\phi^j}{\partial\theta}\right] \tag{41}$$

where $\sigma_r^j(r,\theta,t)$, $\sigma_\theta^j(r,\theta,t)$, and $\sigma_{r\theta}^j(r,\theta,t)$ are radial, tangential, and shearing stresses, respectively.

Within a given layer, the stresses, strains, and displacements in a plane thermoelasticity problem are related as

$$\epsilon_r^j = \left(\frac{1+\nu_j}{E_j}\right)[(1-\nu_j)\sigma_r^j - \nu_j\sigma_\theta^j] + (1+\nu_j)\alpha_j T^j = \frac{\partial u_r^j}{\partial r} \tag{42}$$

$$\epsilon_\theta^j = \left(\frac{1+\nu_j}{E_j}\right)[(1-\nu_j)\sigma_\theta^j - \nu_j\sigma_r^j] + (1+\nu_j)\alpha_j T^j = \frac{1}{r}\left[\frac{\partial u_\theta^j}{\partial\theta} + u_r^j\right] \tag{43}$$

$$\epsilon_{r\theta}^j = \left(\frac{1+\nu_j}{E_j}\right)\sigma_{r\theta}^j = \frac{1}{2r}\left[\frac{\partial u_r^j}{\partial\theta} + r\frac{\partial u_\theta^j}{\partial r} - u_\theta^j\right] \tag{44}$$

where $\epsilon_r^j(r,\theta,t)$, $\epsilon_\theta^j(r,\epsilon,t)$, and $\epsilon_{r\theta}^j(r,\theta,t)$ are the radial, tangential, and shearing strains, respectively, and $u_r^j(r,\theta,t)$ and $u_\theta^j(r,\theta,t)$ are the radial and tangential displacements.

For a J-layered cylindrical structure with a hollow air core (layer 1) where thermal stresses and strains in layer j, $j=2,3,4\ldots,J$, are of interest (a total of $J-1$ stressed layers), there are $4(J-1)$ stress and displacement boundary conditions to be satisfied. Symbolically, they are written as

at $r = r_1$:

$$\sigma_r^2(r,\theta,t) = 0 \tag{45}$$

$$\sigma_{r\theta}^2(r,\theta,t) = 0 \tag{46}$$

at $r = r_j$ $(j=2,3,4,\ldots,J-1)$:

$$\sigma_r^j(r,\theta,t) = \sigma_r^{j+1}(\mathrm{r},\theta,t) \tag{47}$$

$$\sigma_{r\theta}^j(r,\theta,t) = \sigma_{r\theta}^{j+1}(r,\theta,t) \tag{48}$$

$$u_r^j(r,\theta,t) = u_r^{j+1}(r,\theta,t) \tag{49}$$

$$u_\theta^j(r,\theta,t) = u_\theta^{j+1}(r,\theta,t) \tag{50}$$

at $t = r_J$:

$$\sigma_r^J(r,\theta,t) = 0 \tag{51}$$

$$\sigma_{r\theta}^J(r,\theta,t) = 0 \tag{52}$$

where Eqs. (45) and (46) and (51) and (52) indicate no tractions at the bore and the outer surface, respectively, while Eqs. (47) and (48) and (49) and (50) imply continuity of tractions and displacements at the interfaces. Furthermore, the resulting displacements within each layer must also satisfy the single-valuedness condition.

Similarly to the temperature analysis, solutions for the response stresses, strains, and displacements may be obtained

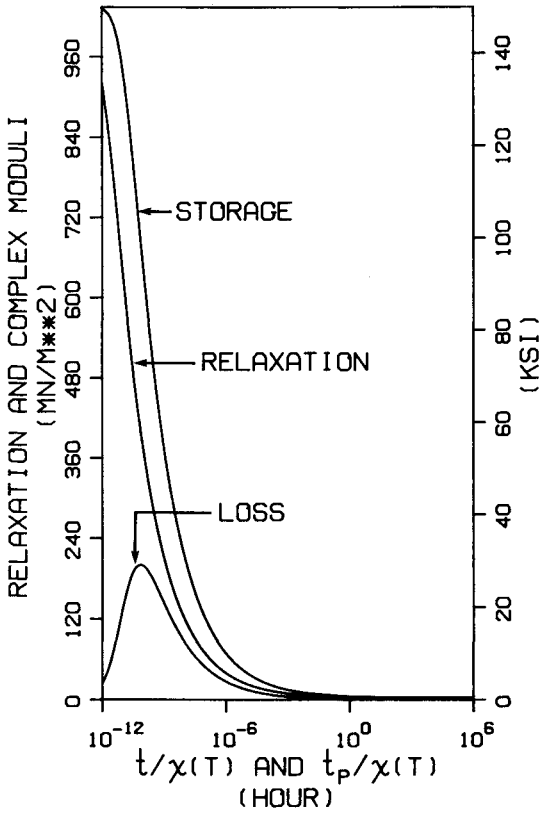

Fig. 5 Variations of relaxation/complex moduli as functions of reduced time/period.

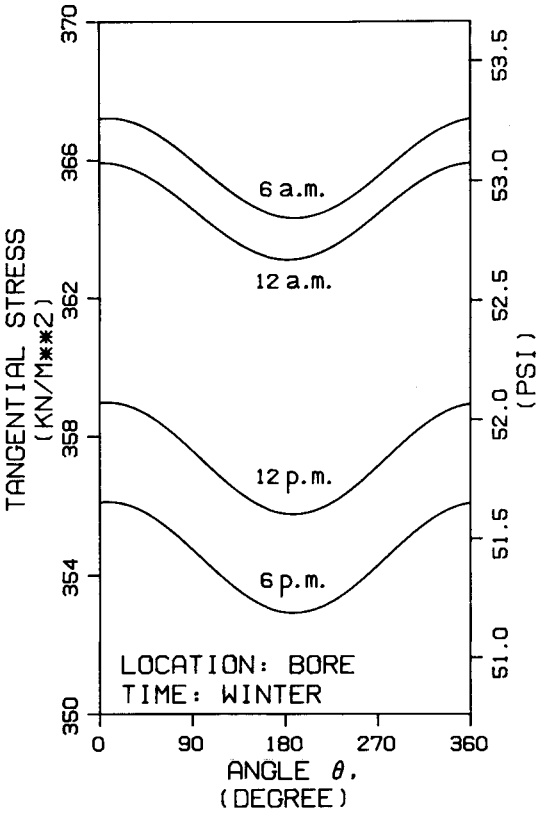

Fig. 6 Circumferential variations of tangential stress at the bore for various hours of a typical winter day at Phoenix, AZ.

in terms of complex frequency-response functions. These solutions can also be found in Ref. 6.

Induced Viscoelastic Stresses

Under the variation of environmental thermal loads, the resulting variation of a strain component at a given point in the propellant can be written as[3]

$$\epsilon(t)=\epsilon_m+\epsilon_c(t)=\epsilon_m+\sum_{k=1}^{K}\epsilon_k e^{i\omega_k t} \tag{53}$$

where ϵ_m is the mean strain induced by the difference between the stress-free temperature, T_f, and the long-term mean temperature, T_m, of the propellant, and $\epsilon_c(t)$ is the steady-state harmonic strain.

Consequently, the corresponding viscoelastic stress variation becomes[3]

$$\sigma(t)=\epsilon_m E(T,t)+\sum_{k=1}^{K}\epsilon_k E^*(\mathrm{T},\omega_k)e^{i\omega_k t} \tag{54}$$

where $E(T,t)$ and $E^*(T,\omega)=E'(T,\omega)+iE''(T,\omega)$ are the relaxation and complex moduli of the propellant. $E'(T,\omega)$ and $E''(T,\omega)$ are referred to as storage and loss moduli, respectively.

The master curve of the relaxation modulus for a propellant is usually written as[4]

$$E(T,t)=E_e+(E_g-E_e)\Big/\left(1+\frac{t}{\tau\chi(T)}\right)^{\eta} \tag{55}$$

where E_g, E_e, τ, and η are the glassy modulus, the relaxed modulus as time approaches infinity, retardation time, and shape parameter, respectively, and their numerical values are shown in Table 2. The viscoelastic shift function, $\chi(T)$, for temperature T with respect to a reference temperature T_r is defined as

$$\log[\chi(T)]=\frac{-C_1(T-T_r)}{C_2+(T-T_r)+C_3(T-T_r)^2} \tag{56}$$

where the constants T_r, C_1, C_2, and C_3 for this specific material are given as 440.0°R (244.4 K), 20.5036, 372.037°R (206.687 K), and 0.00736 1/°R (0.01325 1/K), respectively.[4] Equation (56) becomes the conventional, linear, Williams-Landell-Ferry viscoelastic shift function when C_3 equals zero.[12]

The storage and loss moduli are obtained by performing sine and cosine Fourier transformations of the relaxation modulus.[13] Using the material parameters given in Table 2, the plots of the relaxation modulus as a function of reduced loading time, $t/\chi(T)$, and of the complex modulus as a function of reduced loading period, $t_p/\chi(T)$, are shown in Fig. 5.

Unlike their elastic counterparts, the viscoelastic stress and strain are time- and temperature-dependent quantities. This is a result of the continuous change in the temperature and the relaxation effect of the propellant material. Furthermore, because of the nonuniform temperature distribution, both the relaxation and complex moduli are spatially dependent.

However, except for the region near the canister, both the symmetric and asymmetric temperature variations of the propellant under high-frequency surface loadings, such as a diurnal cycle, were found to be small. Therefore, it will be assumed that these temperature variations have no influence on the relaxation modulus of the propellant.

Because the temperature variation corresponding to an annual cycle is slow, the deviation of temperature across the propellant at a given time is also found to be negligible. Consequently, for the purpose of relaxation modulus calculation, the temperature distribution in the propellant is considered to be uniform and is equal to its instantaneous average value. Furthermore, since the daily temperature variation as a result of an annual cycle is insignificant, the relaxation modulus for a given day is assumed to be constant and its value is evaluated for the daily mean temperature.

For complex modulus calculations, the value of the shift function is evaluated based on the assumption that the propellant is under isothermal loading with its temperature equal to the long-term mean value. The error associated with this

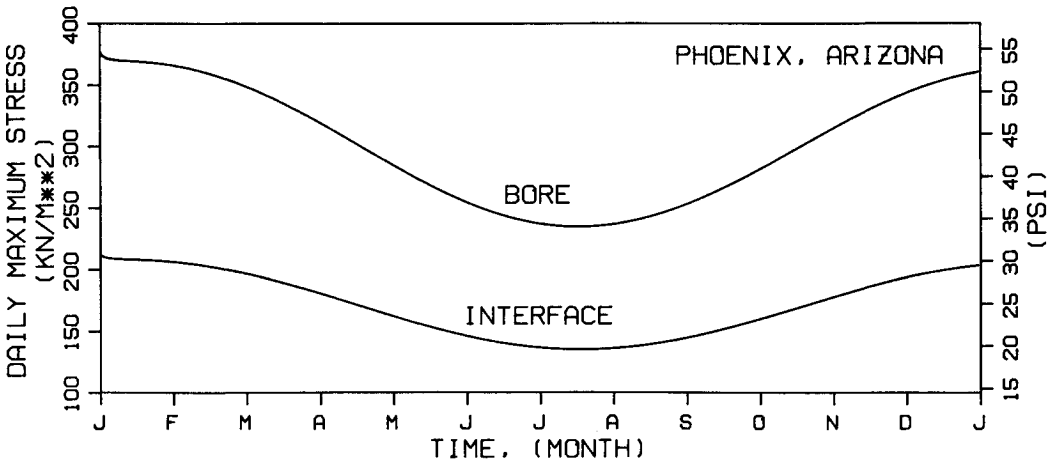

Fig. 7 Yearly variations of daily maximum stresses at the bore and at the interface of the propellant at Phoenix, AZ.

assumption is minimized if the frequency of the effective temperature is relatively small.

The complex frequency-response functions corresponding to elastic solutions may be modified and used to evaluate the response viscoelastic stresses and strains. This can be accomplished by replacing the elastic modulus with the viscoelastic complex modulus for steady harmonic components and with the relaxation modulus for constant stress.[3]

It is assumed in this study that the stress-free and strain-free temperatures are identical because the difference between them is usually small. These temperatures are also assumed to be independent of time and remain constant though slow variations have been observed experimentally.

Using the stress-free temperature shown in Table 2 together with the canister which is assumed to be elastic, Fig. 6 shows the circumferential variations of tangential stresses at the bore (r_1) for various hours of a typical winter day in Phoenix. The annual variations of the daily maximum stresses at the bore and the interface (r_2) are also computed and plotted in Fig. 7.

Conclusion

In the foregoing analysis, procedures have been developed that permit the calculations of surface and interior temperatures in rocket motors subjected to environmental thermal loads with reasonable accuracy. The effects of the ambient temperature, sky radiation, and wind convection on the structure's surface are assumed to be uniform. However, because of the continuous change in the angular position of the sun, the solar radiation input is assumed to be asymmetrically applied to the cylinder's surface.

As a result of the circumferential distribution of surface temperature, thermal stresses are found to be axially asymmetric. The analysis based on plane strain assumptions yields a good approximation to the rather complex state of stress in portions of the motor removed from the two ends. Near the ends, however, a three-dimensional analysis would be required.

It is seen that the effects of asymmetrical heating and cooling are significant near the surface but diminish toward the bore. While surface temperatures may undergo daily variations of 50°F, bore temperatures stay within a 5°F range. As a consequence, bore stress variations are insignificant although interfacial stresses between propellant and casing may have greater variations. These results may be explained by the combination of the low thermal conductivity and the low modulus-viscoelastic nature of the propellant.

The daily maximum stress in the propellant is found to be the tangential stress at the bore with $\theta = 0$. At this point the cylinder's surface receives the least heat energy from the environment, therefore the greatest difference between the material temperature and the stress-free temperature occurs here. The corresponding time for this stress is found to vary slightly from day to day with a mean value centered approximately at 8 a.m.

Although the linearized radiation boundary condition is shown to give a good solution to surface temperature for the problem at hand, special care should be exercised, however, when the approach is applied to problems in general. Due to the highly nonlinear characteristics of the heat energy balance equation between the structure's surface and the surrounding environment, the errors resulting from using the linearized boundary condition to obtain surface temperature may become large, depending on the geometric parameters and thermal properties of both the inner and outer layers of the motor and the nature of the environmental thermal loads.

Acknowledgment

Acknowledgment is given to the U.S. Army Missile Command (USAMICOM), Redstone, AL, for funding this study under Contract DAAK-40-79-C-0231.

References

[1]Heller, R. A., Kamat, M. P., and Singh, M. P., "Probability of Solid Propellant Motor Failure Due to Environmental Temperatures," *Journal of Spacecraft and Rockets*, Vol. 16, May-June 1979, pp. 140-146.

[2]Heller, R. A. and Singh, M. P., "Temperature Distribution in Randomly and Asymmetrically Heated Cylindrical Structures," *High Temperatures and High Pressures*, Vol. 12, 1980,pp. 457-463.

[3]Heller, R. A. and Singh, M. P., "Thermal Storage Life of Solid Propellant Motors," *Journal of Spacecraft and Rockets*, Vol. 20, March-April 1983, pp. 144-149.

[4]Heller, R. A., Singh, M. P., Thangjitham, S., and Zibdeh, H., "Random Probability Techniques for Rocket Motor Service Life Predictions, Vol. I—Statistics of Mechanical Properties, Loads, and Resulting Stresses," U.S. Army Missile Command, Redstone Arsenal, AL, Tech. Rept. RK-CK-84-2, Sept. 1983.

[5]Singh, M. P., Heller, R. A., and Thangjitham, S., "Thermal Stresses in Concentric Cylinders Due to Asymmetric Ambient Temperature Inputs," *Journal of Thermal Stress*, Vol. 7, No. 2, 1984, pp. 183-195.

[6]Thangjitham, S., *Probabilistic Service Life Prediction of Composite Viscoelastic Cylindrical Structures Under Random Outdoor Environment*, Ph.D. Dissertation, Virginia Polytechnic Institute and State University, Blacksburg, VA, Sept. 1984.

[7]*SOLMET, Hourly Solar Radiation-Surface Meteorological Observations*, National Oceanic and Atmospheric Administration, Washington, D. C., Vols. I & II, TD-9724, 1978.

[8]Idso, S. B. and Jackson, R. D., "Thermal Radiation from the Atmosphere," *Journal of Geophysical Research*, Vol. 74, No. 23, 1969, pp. 55-65.

[9]Ulrich, R. D., *Evolution of the NWC Thermal Standard*, Pt. I, Naval Weapons Center, China Lake, CA, NWC TP 4834, 1970.

[10]Timoshenko, S. P. and Goodier, J. N., *Theory of Elasticity*, 3rd Ed., McGraw-Hill Book Co., New York, 1970.

[11]Boley, B. A. and Weiner, J. H., *Theory of Thermal Stress*, John Wiley & Sons, New York, 1960.

[12]Ferry, J. D., *Viscoelastic Properties of Polymers*, 2nd Ed., John Wiley & Sons, New York, 1970.

[13]Christensen, R. M., *Theory of Viscoelasticity*, Academic Press, New York, 1971.